High-Fidelity Simulations of Shock Induced Break-up of Droplets

Ral Bielawski, Venkat Raman
University of Michigan
Ann Arbor, MI, USA

1 Introduction

Shock droplet interactions are found in a wide range of applications ranging from liquid-fueled detonation engines [1, 2, 3, 4, 5], droplet interactions with high-speed vehicles[6, 7, 8] and detonation mitigation[9]. However, the physical understanding and modeling of such multiphase detonations are hampered by a lack of models for droplet break-up shortly after a shock or detonation. Experimental studies of this problem are available [10, 11, 12] but are only able to measure macroscopic properties and cannot resolve the quantitative details at small scales. There are two approaches to studying shock droplet interactions problem in the literature Euler-Lagrangian approaches[1, 2, 3, 4, 5] and liquid resolving approaches[13, 14, 15, 16]. When describing droplets, especially in the form of spray population, Euler-Lagrangian approaches are commonly used, but the predictive capability of these methods is limited by the accuracy of drag, heat transfer, evaporation, and break-up models used to couple the gas and liquid phase [17]. Moreover, such models have been developed mainly for subsonic flows, and the extreme conditions found in shock interactions may render the underlying assumptions invalid. In particular, the droplet break up has not been explored in detail, but this process is critical for successfully modeling liquid-fueled detonation engines.

Due to the high Weber numbers ($> 10^6$) at the relevant velocities and droplet sizes, the break up could be dominated by catastrophic disintegration. However, even that regime occurs at modest values of $We \approx 350$, and the nature of droplet break down at very high Weber numbers could occur through other pathways. For instance, it has been argued [12] that Rayleigh–Taylor instability induced piercing and shear-induced entrainment are the main mechanisms at these conditions. This leads to uncertainty in the ability of the models to capture the break-up at such extreme conditions. In the literature, there are several droplet break up models for the catastrophic breakup regime. The cascade breakup (CAB) model[18] is designed for the catastrophic breakup occurring at Weber numbers greater than 350 but is primarily used in subsonic studies. Numerical studies on a detonation passing through a cloud of water droplets [5] have used the Pilch and Erdman model for break-up time. Another break up model in literature is the shear-induced entrainment model (SIE) Thefanous [12] designed for shock droplet interactions. All three of these models predict different break up times and droplet distributions. Experimental studies conducted on shock-droplet interactions [10, 11, 12] show a large region containing liquid as the droplets break up. To the author's knowledge, there is no work that characterizes the droplet distribution generated by the shock-droplet interactions, which is necessary for validating the break up models.

Since experiments are not yet able to capture the small-scale details of droplet breakup, numerical approaches provide the best possible path forward. There exists a range of methods for studying compressible multi-phase flows, but the diffuse interface approach is followed here [19]. Prior studies on droplet-shock interactions have focused primarily on the trajectory and deformation of the original droplet [11,

Correspondence to: rbielaw@umich.edu

13, 10]. To assess the break up process, the primary droplet mass needs to be tracked in addition to the post-impact droplet structure, including the newly generated droplets arising from the shock interaction. These "shed" droplets and their properties (i,e., size, velocity, and temperature) will affect the post-impact detonation structure.

The current study will use fully-resolved three-dimensional simulations of Mach 3-5 shock interaction with a 100 μm water droplet. The goal is to characterize the post-impact droplet distribution using a novel coloring algorithm. This will allow both the primary droplet and the secondary shed droplets to be tracked. To the author's knowledge, this is the first high-fidelity study of shock-droplet interactions that captures the shed-droplet distribution.

2 Simulation configuration and numerical approach

The computational domain is a rectangular channel with a uniform mesh in each direction containing a 100 μm water droplet in quiescent atmospheric air. An incident shock wave of the chosen speed is sent into the domain through the left boundary, with post-shock conditions patched behind this moving shock. The droplet density is set to $\rho = 998$ kg/m^3, with a surface tension of $\sigma = 72$ mN/s. The viscosity and thermal conductivity of the droplet are assumed to be a constant value of $8.90{*}10^4$ kg/ms and 0.598 W/mK, respectively. Three different incidence shock speeds were computed, including $Ma = 3$, 4, and 5.

A diffuse interface approach is used to capture the multiphase dynamics. The solution is conducted using a two-fluid Eulerian approach[20, 21], where both fluids are captured on the same grid. In the diffuse interface volume of fluid (VOF) approach, the volume fraction, phase-specific mass and internal energy, and the mixture momentum are transported. It is assumed that at the interface, the gas and liquid phases are in equilibrium for the evaluation of pressure and velocity [20, 21]. This description results in the following set of equations when including viscous and surface tension effects:

$$\begin{aligned}
\frac{\partial \alpha_l}{\partial t} + u_j \frac{\partial \alpha_l}{\partial x_j} &= 0, \\
\frac{\partial \rho_l \alpha_l}{\partial t} + \frac{\partial \rho_l \alpha_l u_j}{\partial x_j} &= 0, \\
\frac{\partial \rho_g \alpha_g}{\partial t} + \frac{\partial \rho_g \alpha_g u_j}{\partial x_j} &= 0, \\
\frac{\partial \rho u_i}{\partial t} + \frac{\partial \rho u_i u_j}{\partial x_j} + \frac{\partial p}{\partial x_j} &= 0, \\
\frac{\partial \rho_l \alpha_l e_l}{\partial t} + \frac{\partial \rho_l \alpha_l u_j e_l}{\partial x_j} + u_j \alpha_l \frac{\partial p_l}{\partial x_j} &= -p_i \mu (p_l - p_g), \\
\frac{\partial \rho_g \alpha_g e_g}{\partial t} + \frac{\partial \rho_g \alpha_g u_j e_g}{\partial x_j} + u_j \alpha_g \frac{\partial p_g}{\partial x_j} &= p_i \mu (p_l - p_g), \\
\frac{\partial \left(\rho e + \epsilon_\sigma\right)}{\partial t} + \frac{\partial \rho \left(u_j e + \epsilon_\sigma\right) + u_l \Omega_{lj}}{\partial x_j} + \frac{\partial u_j p}{\partial x_j} &= 0,
\end{aligned} \tag{1}$$

where α_l,α_g, ρ_l, ρ_g, p_l, p_g, e_l, and, e_g, are the liquid volume fraction, gas volume fraction, liquid density, gas density, liquid phase internal energy and gas phase internal energy, respectively. p, e, u_i are the mixture pressure, internal energy, and the i-th component of the mixture velocity. The surface tension tensor, surface tension energy, and viscous stress tensor are given by Ω, ϵ_σ, and τ, respectively.

These equations are implemented in an in-house solver that was built on top of AMReX[22] framework to allow for additive refinement of the grid. The details on the AMR routine is given by Zhang et al. [22]. The details on the discretization and implementation are given by Schmidmayer et al. [21]. The pressure relaxation operator, μ, is taken to be stiff, infinitely fast, and the interface pressure is given by p_i. The details of the relaxation process are outlined by Suarel et al. [20]. Linear limited interpolation of the primitive variables is used for velocity and pressure. Away from the droplet interface, the linear limited interpolation is also used for the interpolation of volume fraction, liquid density, and gas density. To reduce numerical dissipation, a non-linear reconstruction is utilized to represent the liquid-gas interface [23], which represents the liquid gas interface by a hyperbolic tangent profile.

The droplet is initialized by refining the mesh an additional level and then averaging the solution down to the lower adaptive mesh refinement (AMR) level to better approximate the initial condition as a sphere. The computational solution uses six levels of AMR, giving a grid resolution of $400nm$ in liquid-containing regions. The shock structure is refined using up to 4 levels of refinement for a resolution of 1.6 μm. To dynamically track the droplets, a three-dimensional connected component labeling is utilized [24]. Briefly, this algorithm finds contiguous regions of liquid and labels them with a unique ID at each time step. The volume of the regions is determined based on the cell volume and the liquid volume fraction associated with the labeled cells. The droplet radii reported here assumed spherical volumes. For the purpose of identifying droplets, cells with liquid volume fraction smaller than 10^{-3} are labeled as gas phase.

3 Results

Three different time snapshots from the simulation with Mach 3 incident shock are shown in Fig. 1. The earliest time shows the characteristic flatting of the primary droplet with limited shedding of secondary droplets in the size range of $1 - 5\mu$m. It is noted that the grid resolution is 400nm, which implies that droplets smaller than roughly 1 μm are difficult to capture accurately. As the break-up progresses, further shedding of fine and larger droplets can be observed, and instability-induced waves on the droplet surface become prominent. Two other features are apparent, with the parent droplet showing a spike and Rayleigh Taylor piercing (RTP) of the droplet. The droplet spike refers to the liquid region that protrudes from the primary droplet and is the most forward point of this droplet. This feature has been observed in other experiments as well as simulations [11]. This feature (as well as RTP) is present in the Mach 4 incident shock case as well, as shown in Fig. 2. Pronounced ligaments can be seen along the side of the droplets, with secondary droplets shedding from these ligaments through pinching. The Mach 3 and 4 cases are qualitatively similar, with the Mach 4 case showing a more pronounced droplet spike as well as more shed droplets as compared to the Mach 3 case. This trend is followed for the higher speed Mach 5 case, with more droplets generated by the impact process, and also features a stronger droplet spike and RTP.

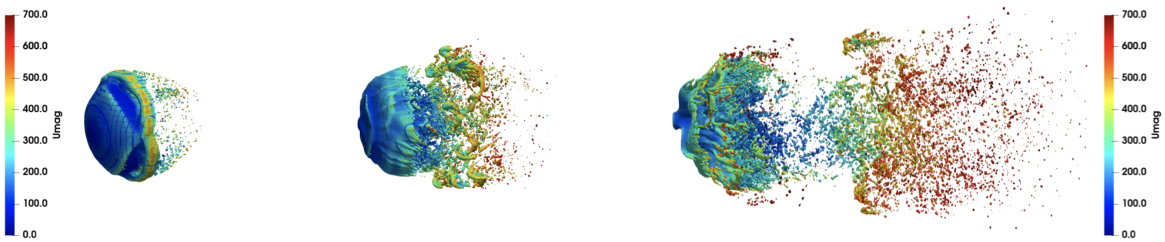

Figure 1: Liquid interface colored by velocity for a 100μm water droplet after impact with a Mach 3 shock as three different times: (Left) $t = 1.4\mu$s (middle) $t = 2.1\mu$s, (right) $t = 2.8\mu$s.

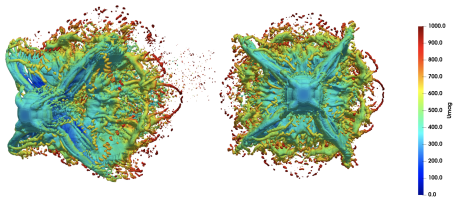

Figure 2: Liquid interface colored by velocity for a 100 μm water droplet after impact with a Mach 4 shock. The piercing of the droplet surface can be seen in 4 locations around the droplet leading to the formation of a droplet-spike.

Finally, the droplet distribution for the three cases is shown in Fig. 3. At early times, it is seen that most of the generated droplets are small for all three cases. After 2μs, additional sizes are generated for all cases, with the higher Mach number cases showing a near continuous generation of small diameter droplets. At 3μs, all cases show a continuous distribution of droplets extending up to 20 μm. While these distributions nearly follow the log-normal profile, the Mach 3 case shows some deviation. However, at later times (not shown here), the profiles are closed to log-normal distribution for all Mach numbers. For the Mach 5 case, it is also seen that the primary droplet breaks down into multiple droplets with diameters ranging from 40-50 μm, generated due to the RTP process.

A preliminary assessment of droplet breakup models is also shown in Fig. 3, through comparison with the SIE model [12]. The SIE model is expressed as

$$\begin{aligned} \frac{m}{m_0} &= \frac{1}{2}\left(1 + cos\pi\frac{T}{3.5}\right), \\ T &= \frac{tU_r}{d_0}\sqrt{\frac{\rho_g}{\rho_l}}, \end{aligned} \tag{2}$$

where m_0, m_{shed}, d_0, t and U_r represent the initial droplet mass and the mass at the non-dimensional time,T, initial droplet diameter, time since impact with shock and the relative velocity, respectively. This model does not give any information about the shed distribution but assumes that the shed-droplet are small. As no size is given, the shed droplets are taken to be 1 μm. The results for the SIE model are plotted in green in Fig. 3. It can be seen that the parent droplet mass shows reasonable agreement with the high-fidelity simulation for the Mach 3 and 4 cases. The Mach 5 case has the parent droplet breaking up due to the piercing, which the SIE model is unable to capture. Further, the assumption that the secondary droplets are small may not be reasonable given the large range of droplet diameters observed in the simulations.

4 Conclusions

High-fidelity simulations of shock-droplet interactions were conducted to estimate the post-impact droplet distribution. AMR-based techniques were used to accurately represent the small droplets shed by the shock impact. The simulations show that droplet flattening, fine droplet mist formation, growth of surface waves, and droplet piercing as qualitative features that agree with prior experiments. The quantitatively measured shed-droplet distribution tends towards a log-normal distribution. The Mach 3 and 4 cases are qualitatively similar, with piercing occurring at four locations and the formation of a droplet spike. In contrast, the Mach 5 case has piercing at a single point, leading to the parent droplet splitting into four parts. The shed droplet distribution is compared to the SIE model and shows relatively good agreement for the amount of shed mass but does not capture the shed droplet distribution very well. This

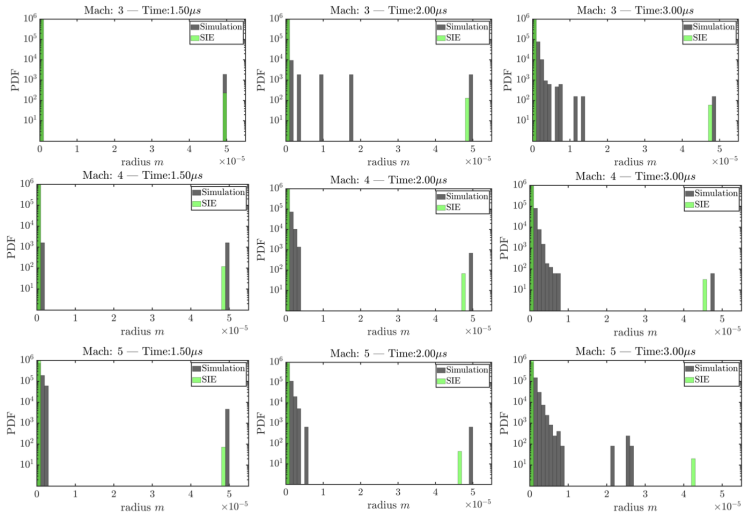

Figure 3: Post-impact droplet distribution for the three simulated cases: (Top) Mach 3, (middle) Mach 4, (bottom) Mach 5. The simulated results are shown in grey and SIE model in green. For the SIE model, the shed mass is assumed to be droplets with a diameter of 1 μm.

work provides vital insights into the droplet distribution that can inform corrections to currently available break-up models. Improvement of the current break-up models is critical for accurately modeling liquid-fueled detonation engines and their realization for power generation or propulsion applications.

References

[1] Supraj Prakash et al. “Three-dimensional Numerical Simulation of Liquid RP-2/O2 based Rotating Detonation Engine”. In: *In Review Combustion and Flame* ().

[2] Qingyang Meng et al. “Eulerian-Lagrangian modelling of rotating detonative combustion in partially prevaporized n-heptane sprays with hydrogen addition”. In: *Fuel* 290 (2021), p. 119808.

[3] VB Nguyen et al. “Numerical investigation of the liquid-fueled pulse detonation engine for different operating conditions”. In: *Shock Waves* 29 (2019), pp. 1205–1225.

[4] Jiasen Wang et al. “Numerical study on atomization and evaporation characteristics of preheated kerosene jet in a rotating detonation scramjet combustor”. In: *Applied Thermal Engineering* 203 (2022), p. 117920.

[5] Yong Xu, Majie Zhao, and Huangwei Zhang. “Effect of water droplet breakup on hydrogen/air detonations”. In: *International Conference on Liquid Atomization and Spray Systems (ICLASS)*. Vol. 1. 1. 2021.

[6] Andrew Hess et al. “Evaluation of droplet aerodynamic breakup models in supersonic and hypersonic flows”. In: *AIAA Scitech 2021 Forum*. 2021, p. 0751.

[7] Bruce Moylan, Brian Landrum, and Gerald Russell. “Investigation of the physical phenomena associated with rain impacts on supersonic and hypersonic flight vehicles”. In: *Procedia Engineering* 58 (2013), pp. 223–231.

[8] Hassan Beydoun et al. “Realistic Weather Modeling for Hypersonic Vehicles: Raindrop Shock Interactions”. In: *ASCEND 2021*. 2021, p. 4230.

[9] Hiroaki Watanabe et al. “Numerical investigation on propagation behavior of gaseous detonation in water spray”. In: *Proceedings of the Combustion Institute* 37.3 (2019), pp. 3617–3626.

[10] Sergey V Poplavski et al. “On the interaction of water droplet with a shock wave: Experiment and numerical simulation”. In: *International Journal of Multiphase Flow* 127 (2020), p. 103273.

[11] David Hébert et al. “Investigation of mechanisms leading to water drop breakup at Mach 4.4 and Weber numbers above 10 5”. In: *SN Applied Sciences* 2 (2020), pp. 1–23.

[12] TG Theofanous and GJ Li. “On the physics of aerobreakup”. In: *Physics of fluids* 20.5 (2008), p. 052103.

[13] Benedikt Dorschner et al. “On the formation and recurrent shedding of ligaments in droplet aerobreakup”. In: *Journal of Fluid Mechanics* 904 (2020), A20.

[14] JC Meng and T Colonius. “Numerical simulations of the early stages of high-speed droplet breakup”. In: *Shock waves* 25 (2015), pp. 399–414.

[15] Daniel P Garrick, Wyatt A Hagen, and Jonathan D Regele. “Secondary atomization of liquid columns in compressible crossflows”. In: *arXiv preprint arXiv:1906.04307* (2019).

[16] Georgia Nykteri and Manolis Gavaises. “Droplet aerobreakup under the shear-induced entrainment regime using a multiscale two-fluid approach”. In: *Physical Review Fluids* 6.8 (2021), p. 084304.

[17] William A Sirignano. “Fuel droplet vaporization and spray combustion theory”. In: *Progress in Energy and Combustion Science* 9.4 (1983), pp. 291–322.

[18] Franz X Tanner. “Development and validation of a cascade atomization and drop breakup model for high-velocity dense sprays”. In: *Atomization and sprays* 14.3 (2004).

[19] Richard Saurel and Carlos Pantano. “Diffuse-interface capturing methods for compressible two-phase flows”. In: *Annual Review of Fluid Mechanics* 50 (2018), pp. 105–130.

[20] Richard Saurel et al. “A relaxation-projection method for compressible flows. Part I: The numerical equation of state for the Euler equations”. In: *Journal of Computational Physics* 223.2 (2007), pp. 822–845.

[21] Kevin Schmidmayer et al. “A model and numerical method for compressible flows with capillary effects”. In: *Journal of Computational Physics* 334 (2017), pp. 468–496.

[22] Zhang et al. “AMReX: A Framework for Block-Structured Adaptive Mesh Refinement”. In: *Journal of Open Source Software* 4.37 (2019), p. 1370.

[23] Daniel P Garrick, Wyatt A Hagen, and Jonathan D Regele. “An interface capturing scheme for modeling atomization in compressible flows”. In: *Journal of Computational Physics* 344 (2017), pp. 260–280.

[24] Martin Heinrich and Rüdiger Schwarze. “3D-coupling of Volume-of-Fluid and Lagrangian particle tracking for spray atomization simulation in OpenFOAM”. In: *SoftwareX* 11 (2020), p. 100483.